Comparison of Performances of Electrical Impedance Tomography Evaluated with 2-D and 3-D Models

Jean-François Chateaux and Mustapha Nadi, *Member, IEEE*

***Abstract*—This paper describes electrical impedance tomography (EIT) sensitivity evaluation using two models. The first is the classical circular two-dimensional (2-D) model used by past authors. The second is a three-dimensional (3-D) cylindrical model, which takes into account the height of the object under study. Having reported the analytical expression of the potential field of the 2-D model, we derive an equivalent solution for the 3-D case. Having analyzed the convergence of the solutions, we compute for different conductivity perturbations the ratio of the sensitivities obtained with the two models. Results indicate that the 2-D model, as compared with the 3-D model, generally overestimates sensitivity by a factor of two unless the conductivity perturbation is extensive and more conductive than the principal medium. In such a case, the 2-D model tends to underestimate EIT sensitivity.**

***Index Terms*—Biomedical engineering, biomedical impedance imaging, electromagnetic fields, error analysis, simulation.**

I. Introduction

ELECTRICAL impedance tomography (EIT) is an imaging method reconstructing conductivity and/or permittivity distribution in a slice through the body [1]. Data are collected noninvasively by means of impedance measurements at frequencies up to 1 MHz [2]. Since the first impedance tomography, obtained in 1982 by Brown and Barber [3], many clinical applications were and are still being investigated such as breast tumor imaging [4], hyperthermia monitoring [5], or gastric emptying monitoring [6]. Most of the biomedical applications are under investigation and numerous teams are concerned worldwide [7]. The technique's theoretical performance have been studied by Isaacson [8] and Seagar *et al.* [9], the latter having defined the concept of sensitivity, resolution, and contrast as related to EIT. Both have used a two-dimensional (2-D) model, i.e., a disc with a circular conductivity perturbation. Nevertheless, unlike classical tomography devices (e.g., X-ray tomographs), images are adversely affected by out-of-plane objects as currents injected for impedance measurement do not remain confined to this plane. Since the 2-D model does not take the phenomenon into account, the aim of this paper is to estimate the limitations of the 2-D model by comparing the results obtained with a three-dimensional (3-D) model.

Manuscript received November 12, 1999; revised May 3, 2000.

The authors are with the Faculté des Sciences, Laboratoire d'Instrumentation Electronique de Nancy, University Henri POINCARE, 54506 Vandoeuvre-les-Nancy, France.

Publisher Item Identifier S 0018-9480(00)09538-7.

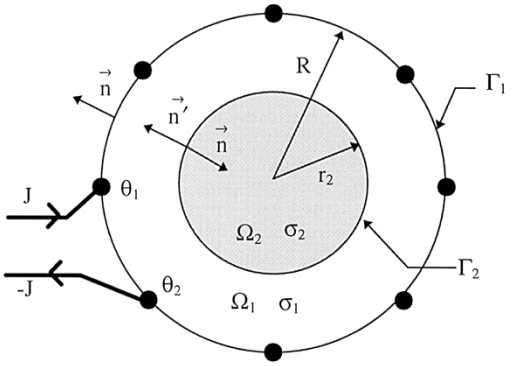

Fig. 1. 2-D (heterogeneous) model, adjacent injecting mode, eight electrodes.

II. Numerical Models

A. 2-D Model

Two different numerical models are compared, *viz*. a 2-D and 3-D one. Each of these models can be homogeneous or heterogeneous, depending on the presence or nonpresence of a central conductivity perturbation. The purpose of the models is to evaluate the capability of an EIT system to detect the presence of a conductivity perturbation to determine EIT sensitivity.

In the 2-D case (Fig. 1), the computational domain is a disc Ω_1 with a boundary Γ_1, radius R, and uniform conductivity $\sigma_1(S \cdot m^{-1})$. In the heterogeneous case, a central circular conductivity perturbation Ω_2 with a boundary Γ_2, radius r_2, and conductivity σ_2 $(S \cdot m^{-1})$ is added. A set of electrodes, usually 16 or 32, is attached to Γ_1. Two of these electrodes are used for current injection through boundary Γ_1. The remaining electrodes measure the potential profile along Γ_1. Depending on the angular positions θ_1 and θ_2 of the two injecting electrodes, one can differentiate the following two configurations:

- adjacent injecting mode, where the two current electrodes are side by side;
- polar injecting mode, where these two electrodes are 180° apart.

B. Extension to 3-D Model

With the 3-D model (Fig. 2), the discs of the 2-D model are replaced with cylinders with a height H, which results in a coaxial setup. As the boundaries Γ_1 and Γ_2 become surfaces, the potential field generated by the current electrodes can extend out of the plane of the electrodes. Previous computations have shown that the potential field in Ω_1 and Ω_2 differs greatly when computed with the 2-D or 3-D model.

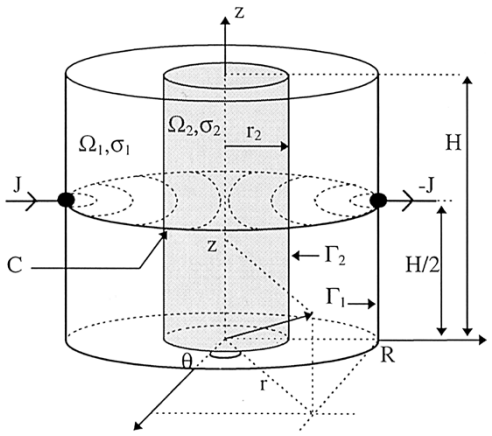

Fig. 2. 3-D (heterogeneous) model, polar injecting mode.

III. Computation of Potential Profiles

A. EIT Performance Evaluation Method

In order to evaluate EIT sensitivity to the presence of conductivity heterogeneity, the potential along boundary Γ_1 in both homogeneous and heterogeneous cases is computed. The potential profile obtained in the homogeneous case is used as a reference and any difference between this reference and the profile obtained with the heterogeneous model is caused by the perturbation Ω_2.

Calling ϕ_{Γ_1} the potential profile along boundary Γ_1, an analytical description of ϕ_{Γ_1} can be obtained because of the axial symmetry of the problem. Such an analytical solution has the following two main advantages over a numerical one.

- Computations are generally much faster, as an iterative process is not necessary. Moreover, the potential may be computed just at the points that are of interest.
- An analytical solution contains more information on system behavior.

B. 2-D Problem Derivation

With these notations and in the 2-D case (Fig. 1), the problem can be formulated as

$$\begin{cases} \nabla^2\phi(r,\,\theta) = 0 & (1) \\ -\sigma_1 \cdot \dfrac{\partial\phi_1(r,\,\theta)}{\partial\vec{n}}\Big|_{r=R} = J \cdot \big[\delta(\theta-\theta_1) - \delta(\theta-\theta_2)\big] & (2) \\ -\sigma_1 \cdot \dfrac{\partial\phi_1(r,\,\theta)}{\partial\vec{n}}\Big|_{r=r_2} = \sigma_2 \cdot \dfrac{\partial\phi_2(r,\,\theta)}{\partial\vec{n}'}\Big|_{r=r_2} & (3) \\ \phi_1(r_2,\,\theta) = \phi_2(r_2,\,\theta) & (4) \end{cases}$$

where ϕ_1 and ϕ_2 are, respectively, the potential through Ω_1 and Ω_2, J is the current density ($A \cdot m^{-1}$) and δ is the Dirac delta function. Of course, when computing potential in the homogeneous case ($\sigma_2 = \sigma_1$), (3) and (4) have no signification. The problem is solved by the classical method of variable separation. Variable r, which gives the radial position of a point is set to $r = R$ because only the potential along boundary Γ_1 is of interest. Details about the derivation of the problem can be found in [8], and one obtains on the Γ_1 boundary

$$\phi_{\Gamma_1}(\theta) = -\sum_{n=1}^{\infty} \frac{J\cdot R}{\sigma_1 \cdot n\pi} \cdot P_n(\alpha,\,\beta) \cdot\big[C_n\cos(n\theta) + S_n\sin(n\theta)\big] \quad (5)$$

within the homogeneous case $P_n(\alpha,\,\beta) = 1$, and within the heterogeneous case

$$P_n(\alpha,\,\beta) = \frac{1 - \dfrac{\alpha-1}{\alpha+1}\cdot\beta^{2n}}{1 + \dfrac{\alpha-1}{\alpha+1}\cdot\beta^{2n}}.$$

In both cases, C_n and S_n are given by

$$C_n = \cos(n\theta_1) - \cos(n\theta 2) \quad S_n = \sin(n\theta_1) - \sin(n\theta 2)$$

and $(\alpha,\,\beta)$ are defined in Section III-D.

C. 3-D Problem Derivation

In the 3-D model, computations were extended to a cylinder of a height H. Boundaries Γ_1 and Γ_2 become surfaces. In order to simplify the derivation of the problem, a Dirichlet condition is chosen for the top and bottom of cylinder, applying a zero potential to these surfaces. Dimension H should be large for these boundaries conditions to be realistic. Then, with the same notations as in the 2-D case, the problem can be formulated as

$$\begin{cases} \nabla^2\phi(r,\,\theta,\,z) = 0 & (6) \\ -\sigma_1 \cdot \dfrac{\partial\phi_1(r,\,\theta,\,z)}{\partial\vec{n}}\Big|_{r=R} = J \cdot \big[\delta(\theta-\theta_1) - \delta(\theta-\theta_2)\big] & (7) \\ -\sigma_1 \cdot \dfrac{\partial\phi_1(r,\,\theta,\,z)}{\partial\vec{n}}\Big|_{r=r_2} = \sigma_2 \cdot \dfrac{\partial\phi_2(r,\,\theta,\,z)}{\partial\vec{n}'}\Big|_{r=r_2} & (8) \\ \phi_1(r_2,\,\theta,\,z) = \phi_2(r_2,\,\theta,\,z) & (9) \\ \phi(r,\,\theta,\,0) = \phi(r,\,\theta,\,H) = 0. & (10) \end{cases}$$

Equations (8) and (9) are specific to the heterogeneous problem. As we can observe in Fig. 2, the electrodes are located at height $H/2$ along contour C. Computational details are given in the Appendix, and one obtains for the potential profile along the C contour in the homogeneous case

$$\phi_C^{\mathrm{Hom}}(\theta) = -\frac{4J}{\sigma_1\pi H}\sum_{n=1}^{\infty}\sum_{m=1}^{\infty}\big[C_n\cos(n\theta) + S_n\sin(n\theta)\big] \cdot\sin\left(\frac{m\pi}{2}\right)\cdot\frac{I_n\left(\dfrac{m\pi}{H}R\right)}{\lambda_{nm}} \quad (11)$$

with

$$\lambda_{nm} = \frac{\partial I_n\left(\dfrac{m\pi}{H}r\right)}{\partial r}\Big|_{r=R} = \frac{n}{R}\,I_n\left(\frac{m\pi R}{H}\right) + \frac{m\pi}{H}\,I_{n+1}\left(\frac{m\pi R}{H}\right)$$

where I_n is the modified Bessel's function of the first kind and order n, and in the heterogeneous case

$$\phi_C^{\mathrm{Het}}(\theta) = -\frac{4J}{\sigma_1 \pi H} \sum_{n=1}^{\infty} \sum_{m=1}^{\infty} \left[C_n \cos(n\theta) + S_n \sin(n\theta)\right] \cdot \sin\left(\frac{m\pi}{2}\right) \cdot \frac{I_n\left(\frac{m\pi}{H} R\right) - \gamma \cdot I_n\left(\frac{m\pi}{H} \frac{r_2^2}{R}\right)}{\lambda_{nm} + \gamma \cdot \mu_{nm}} \tag{12}$$

with

$$\gamma = \frac{\alpha - 1}{\alpha + 1}$$

and

$$\mu_{nm} = \frac{m\pi r_2^2}{HR^2} \left[\frac{nHR}{m\pi r_2^2} I_n\left(\frac{m\pi}{H} \frac{r_2^2}{R}\right) + I_{n+1}\left(\frac{m\pi}{H} \frac{r_2^2}{R}\right)\right].$$

D. 3-D Parameters Evaluated For Comparison Purposes

According to Seagar *et al.* [9], the contrast α, resolution β, and sensitivity S are defined as follows:

- contrast:

$$\alpha = \sigma_2/\sigma_1$$

- resolution:

$$\beta = r_2/R$$

- sensitivity:

$$S = \sqrt{\frac{1}{2\pi} \int_0^{2\pi} \left(\phi_{\mathrm{Hom}}(\theta) - \phi_{\mathrm{Het}}(\theta)\right)^2 d\theta}.$$

Contrast and resolution are then parameters describing the domain's level of nonhomogeneity. Sensitivity appears as the quadratic mean of the difference between potential profiles calculated in the homogeneous case ($\sigma_2 = \sigma_1$) and heterogeneous case ($\sigma_2 \neq \sigma_1$). This provides a value for the alteration of the potential profile along Γ_1 (or C) due to the presence of perturbation Ω_2. Of course, $\phi_{\Gamma_1}^{\mathrm{Het}}(\theta)$ is dependent on contrast and resolution, and sensitivity S is also a function of α and β.

IV. Results

A. Convergence Speed

Practical computation of $\phi_{\Gamma_1}(\theta)$, i.e., the potential profile along Γ_1 in the 2-D case, shows that convergence depends on resolution β: convergence is slower when β approaches unity. Nevertheless, when $\beta = 0.9$, the first 20 terms of the sum giving $\phi_{\Gamma_1}(\theta)$ suffice. With the 3-D model, a similar phenomenon is observed, but convergence is much slower. In (11) and (12), involving infinite sum, we have taken in practice $n\max = 70$, i.e., the first 70 orders of the modified Bessel's function, and $m\max = 4000$ when $\beta = 0.9$.

B. Computational Results

We performed computations using 16 electrodes along Γ_1 in the 2-D case and along the C contour in the 3-D case. The radius R of Ω_1 injected current density J and conductivity σ_1 were taken as equal to one.

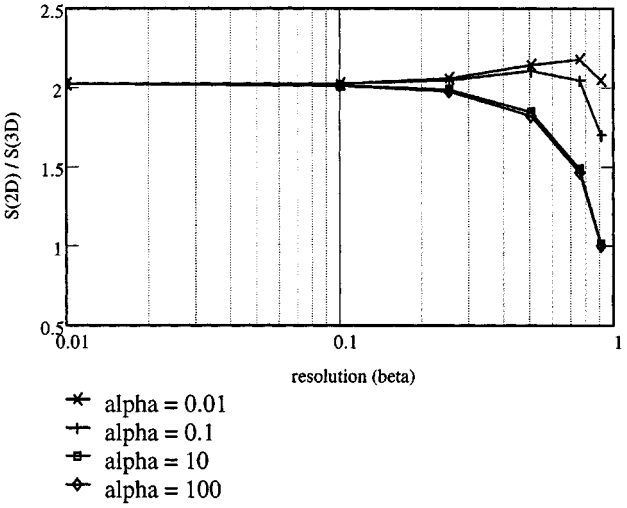

Fig. 3. ROS versus resolution β in polar injecting mode.

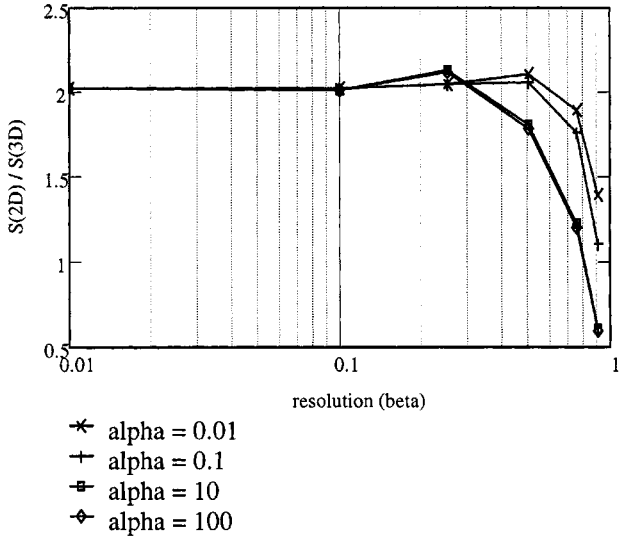

Fig. 4. ROS versus resolution β in adjacent injecting mode.

In order to compare the sensitivities evaluated by the two models, we used the ratio of sensitivity computed with the 2-D model over the sensitivity obtained with the 3-D model. Computation for various contrast values α ranging from 0.01 to 100 were performed to simulate the dynamic commonly encountered in body imaging. Resolution β ranges from 0.01 to 0.9. Computation is limited to $\beta = 0.9$ because of the dependence on the speed of convergence to β.

For the polar injecting mode, Fig. 3 gives the $S_{2D}(\alpha, \beta)/S_{3D}(\alpha, \beta)$ ratio, i.e., the ratio of sensitivities (ROS), for four different values of α. The same computations are made in the adjacent current injecting mode, and Fig. 4 presents the results obtained in this case.

V. Discussion and Conclusion

It clearly appears that the ROS calculated with the two models depends on the contrast and resolution values. In both the polar

and adjacent modes, the ROS decreases when contrast α and resolution β increase. When β is small, i.e., near the homogeneous case, the 2-D model tends to overestimate EIT sensitivity (as compared to the 3-D model) by a factor close to two. When β increases, overestimation drops to become less than unity when perturbation Ω_2 is more conductive than Ω_1 ($\alpha > 1$). In this case, the 2-D model will underestimate EIT sensitivity, especially in the adjacent injecting mode.

One can conclude that if the radius of the central conductivity perturbation is small ($\beta \leq 0.1$), the sensitivity predicted by the 2-D model should be divided by two. Of course, the precise value of this correction factor is valid only for a central circular perturbation. In actual practice, this never occurs, but the 2-D model nevertheless provides a good approximation of sensitivity overestimation. The possibility to use the 2-D model is interesting compared to the 3-D model. Indeed, convergence of the 2-D model is much faster and requires less computation time. Moreover, as regards 2-D formulation, it appears that the influence of the conductivity perturbation (Ω_2) is fully included in a single simple term ($P_n(\alpha, \beta)$). Analysis would then be much easier than with the complex 3-D formulation.

Appendix

With the 3-D model, and with the presence of heterogeneity Ω_2, the problem can be expressed through the following set of equations:

$$\begin{cases} \nabla^2\phi(r,\theta,z) = 0 & \text{(A1)} \\ -\sigma_1 \cdot \dfrac{\partial\phi_1(r,\theta,z)}{\partial\vec{n}}\Big|_{r=R} = J \cdot \left[\delta(\theta-\theta_1) - \delta(\theta-\theta_2)\right] & \text{(A2)} \\ -\sigma_1 \cdot \dfrac{\partial\phi_1(r,\theta,z)}{\partial\vec{n}}\Big|_{r=r_2} = \sigma_2 \cdot \dfrac{\partial\phi_2(r,\theta,z)}{\partial\vec{n}'}\Big|_{r=r_2} & \text{(A3)} \\ \phi_1(r_2,\theta,z) = \phi_2(r_2,\theta,z) & \text{(A4)} \\ \phi(r,\theta,0) = \phi(r,\theta,H) = 0. & \text{(A5)} \end{cases}$$

In order to cancel Dirac distribution δ, the right-hand-side term of (A2) is expanded along the Γ_1 surface using the Fourier series. This leads to an expression involving a double sum and enforces periodicity along the z axis.

A solution to (A1) is found using the classical method of variable separation

$$\phi(r,\theta,z) = R(r)\cdot\Theta(\theta)\cdot Z(z).$$

Taking the $\Theta(\theta)$ and $Z(z)$ periodical due to a current distribution Fourier expansion, one obtains

$$r^2R'' + rR' - (k^2r^2 + n^2)R = 0 \qquad \text{(A6)}$$

where $-k^2$ and $-n^2$are the constants of separation about $Z(z)$ and $\Theta(\theta)$, respectively. R'' and R' are second and first derivatives with respect to variable r. One recognizes in (A6) a nonstandard form of a Bessel's equation using modified (or hyperbolic) Bessel's functions as solutions. We then have

$$R(r) = \begin{cases} I_n(k\cdot r) \\ K_n(k\cdot r) \end{cases}$$

where I_n is the modified Bessel's function of the first kind and order n, whereas K_n is the modified Bessel's function of the second kind. With K_n becoming infinite on zero and the domain of calculus containing the origin, we do not conserve K_n.

Due to (A5) forcing the potential to null on the top and bottom of the cylinder, and because of the periodicity imposed by the current density Fourier expansion, one has

$$Z(z) = \sin(k\cdot z), \qquad \text{with} \quad k = \frac{m\cdot\pi}{H} \qquad \text{(A7)}$$

with m being an integer.

One deduces from (A7) that the current density should be made periodical along the z-axis according to an odd function. Now, by deriving the Fourier expansion of current density distribution on Γ_1, one obtains

$$J(\theta,z) = \frac{2J}{\pi H}\sum_{n=1}^{\infty}\sum_{m=1}^{\infty}\left[C_n\cos(n\theta) + S_n\sin(n\theta)\right] \cdot \sin\left(\frac{m\pi}{2}\right)\sin\left(\frac{m\pi}{H}z\right).$$

We now have all the elements required for the resolution of the homogeneous problem, and the potential on the C contour is then given by (11).

To solve the heterogeneous problem, one tries a solution of the form [10]

$$\begin{cases} \phi_1(r,\theta) = \phi_0(r,\theta) - \gamma\cdot\phi_0\left(\dfrac{r_2^2}{r},\theta\right) \\ \phi_2(r,\theta) = (1-\gamma)\cdot\phi_0(r,\theta) \end{cases} \qquad \text{(A8)}$$

where γ is a constant and ϕ_0 is the potential computed in the homogeneous case. This solution has the advantage of ensuring that (A4) is verified. We then find (12), which gives the potential on the C contour for the heterogeneous case.

References

[1] B. Rigaud and J. P. Morucci, "Bioelectrical impedance techniques in medicine—Part III: Impedance imaging," *Crit. Rev. Biomed. Eng.*, vol. 24, pp. 467–597, 1996.

[2] P. Riu, J. Rosell, and R. Pallas-Areny, "Measurement of frequency behavior of tissue impedance using multifrequency tomography," in *Proc. 8th ICEBI*, Kuopio, Finland, 1992, pp. 127–129.

[3] B. H. Brown and B. C. Barber, "Applied potential tomography—A new *in vivo* medical imaging technique," *Clin. Phys. Physiol. Meas.*, vol. 4, no. 1, 1982.

[4] A. Nowakowski, J. Wtorek, and J. Stelter, "Technical University of Gdansk electroimpedance mammograph," in *Proc. 9th Int. Elect. Bio-Impedance Conf.*, Heidelberg, Germany, 1995, pp. 434–435.

[5] J. Conway, S. Hawley, A. D. Seager, B. H. Brown, and D. C. Barber, "Applied potential tomography (APT) for noninvasive thermal imaging during hyperthermia treatment," *Electron. Lett.*, vol. 21, no. 19, pp. 836–838, 1985.

[6] Y. F. Mangnall, A. J. Baxter, R. Avill, N. C. Bird, B. H. Brown, D. C. Barber, A. D. Seager, A. G. Johnson, and N. W. Read, "Applied potential tomography: A new noninvasive technique for assessing gastric function," *Clin. Phys. Physiol. Meas.*, vol. 8, pp. 119–129, 1987.

[7] *Proc. 10th Int. Elect. Bio-Impedance Conf.*, Barcelona, Spain, Apr. 5–9, 1998.

[8] D. Isaacson, "Distinguishability of conductivities by electric current computed tomography," *IEEE Trans. Med. Imag.*, vol. MI-5, pp. 91–95, MONTH 1986.
[9] A. D. Seagar, D. C. Barber, and B. H. Brown, "Theoretical limits to sensitivity and resolution in impedance imaging," *Clin. Phys. Physiol. Meas.*, vol. 8, pp. 13–31, 1987.
[10] E. Durand, *Electrostatique (III) Methodes de Calculation Dielectriques*. Paris, France: Masson, 1996, p. 237.
[11] U. Baysal and B. M. Eyüboglu, "Use of *a priori* information in estimating tissue resistivities—Application to measured data," *Phys. Med. Biol.*, vol. 44, pp. 1677–1689, 1999.
[12] B. Blade, P. Wende, and K. Lindström, "Two-dimensional electrical impedance profile imaging," *Innov. Tech. Biol. Medicine*, vol. 20, no. 3, pp. 159–167, 1999.
[13] M. L. Boas, *Mathematical Methods in the Physical Sciences*, 2nd ed. New York: Wiley, 1996.

Jean-François Chateaux was born on May 5, 1972, in Clermont Ferrand, France. He received the D.E.A. (Masters) degree in electrical engineering from the University Henri POINCARE, Vandoeuvre-les-Nancy, France, in 1994, and will present his Ph.D. dissertation at the same university in November 2000.

He is currently an Assistant in biomedical instrumentation at the University Henri POINCARE, where he is involved with bioimpedance measurement and bioelectromagnetism research.

Mustapha Nadi (M'87) was born October 14, 1957, in Marrakech, Morocco.

He is currently a Professor in the Electrical Engineering Department, University Henri POINCARE, Vandoeuvre-les-Nancy, France. He is also the Director of the Laboratoire d'Instrumentation Electronique de Nancy (LIEN), University Henri POINCARE, where his research area is on the electronic instrumentation related to biomedical application, bioelectromagnetism, nonlinear ultrasound, and bioimpedance spectroscopy. He is considered an expert in international organizations such as the European Community and the World Health Organization (WHO).

Prof. Nadi is a member of the European Bioelectromagnetic Association (EBEA).